Available online at www.sciencedirect.com
ScienceDirect
Combustion and Flame 155 (2008) 370–379
Combustion and Flame
www.elsevier.com/locate/combustflame

Investigation of autoignition under thermal stratification using linear eddy modeling

M. Oevermann [a,*], H. Schmidt [b], A.R. Kerstein [c]

[a] Technische Universität Berlin, Institut für Energietechnik, Fasanenstr. 89, 10623 Berlin, Germany
[b] Freie Universität Berlin, Institut für Mathematik, Arnimallee 6, 14195 Berlin, Germany
[c] Combustion Research Facility, Sandia National Laboratories, Livermore, CA 94551-0969, USA

Received 1 February 2008; received in revised form 20 April 2008; accepted 29 April 2008

Available online 5 June 2008

Abstract

The influence of thermal stratification on autoignition at constant volume and high pressure is investigated under turbulent conditions using the one-dimensional linear eddy model (LEM) and detailed hydrogen/air chemistry. Results are presented for the influence of initial temperature inhomogeneities on the heat release rate and the relative importance of diffusion and chemical reactions. The predicted heat release rates are compared with heat release rates of recent published studies obtained by two-dimensional direct numerical simulations (DNS). Using the definition of Chen et al. [Combust. Flame 145 (2006) 145–159] for the displacement speed of the H_2 mass fraction tracked at the location of maximum heat release, and a comparison of budget terms, different combustion modes including ignition-front propagation and deflagration waves are identified and the results are compared to the DNS data. The LEM approach shows qualitatively and quantitatively reasonable agreement with the DNS data over the whole range of investigated temperature fluctuations. The results presented in this work suggest that LEM is a potential candidate as a submodel for CFD calculations of HCCI engines.

Keywords: HCCI; Autoignition; Thermal explosion; Turbulence; Linear eddy model

1. Introduction

Homogeneous-charge compression-ignition (HCCI) engines have potentially higher thermal efficiencies and lower NO_x and soot emissions than conventional spark-ignition and Diesel engines, respectively. Compared to conventional compression-ignition (CI) engines, HCCI engines operate under lean conditions with fuel and air well mixed before entering the cylinder. Although major progress has been made, HCCI engines suffer from high carbon monoxide (CO) and unburned hydrocarbon (UHC) emissions. In order to achieve low NO_x emissions, HCCI engines usually operate with very lean fuel/air mixtures and/or exhaust gas recirculation (EGR) to keep peak temperatures low. However, such low temperature levels favor incomplete combustion and high CO levels. Another major problem in the design of HCCI engines is the control of the very high heat release rates, which may cause excessively rapid pressure rise under perfectly homogeneous conditions. One method for reducing

* Corresponding author.
E-mail address: michael.oevermann@tu-berlin.de (M. Oevermann).

0010-2180/$ – see front matter
doi:10.1016/j.combustflame.2008.04.020

the maximum heat release rate is the introduction of thermal or mixture inhomogeneities. Temperature inhomogeneities will lead to some hot and some cold spots, each having different ignition delay times. The hottest spots will ignite first, followed by the colder areas, leading to a spreading of the heat release over a range of crank angles. Ignited and unignited spots build up large temperature gradients between burned and unburned gases where turbulent and molecular mixing become important and cannot be neglected.

In recent direct numerical simulation (DNS) studies [1,2], it has been demonstrated that both ignition fronts and deflagration-like fronts may be present under thermal stratification under HCCI-like conditions. With increasing stratification, the subtle interaction between turbulent mixing and chemistry becomes increasingly important and needs to be taken into account in computational models of HCCI engines. Cook et al. [3] presented a one-dimensional flamelet-type model in enthalpy space capable of capturing HCCI combustion in both relevant regimes identified in the DNS simulation. The model offers the potential for use as a combustion model for CFD calculations of HCCI engines. However, for closure, the enthalpy-based flamelet model needs a probability density function (PDF) for enthalpy and a model for the enthalpy dissipation rate. Using those data directly from the DNS [3], the enthalpy flamelet model was able to achieve good agreement with the DNS results.

Steeper et al. [4] applied the linear eddy model as a stand-alone tool for the investigation of spatial fuel distribution under typical HCCI conditions. They used a simple two-step, six-species chemical mechanism for n-heptane, which was not able to capture the characteristic low-temperature heat release of n-heptane. The authors presented some interesting qualitative results with the LEM; however, they did not make any quantitative comparison with experimental data or other numerical modeling approaches.

In this work we use the linear eddy model (LEM) [5] to investigate the influence of thermal stratification on autoignition under HCCI conditions and compare the results with recent DNS data of Hawkes and coworkers [1,2]. The (one-dimensional) LEM is capable of representing the turbulence–chemistry interaction on all temporal and spatial scales. In comparison to the flamelet-based modeling of Cook et al. [3], the LEM approach after calibration does not need additional input for closure. The predicted heat release rates and the relative importance of reaction and diffusion terms agree reasonably well with the DNS results. The simple one-dimensional model is capable of capturing the key combustion characteristics for the combustion regime of spontaneous ignition fronts, for the deflagration-dominated case, and last for the mixed one. The 1D strategy enables parametric studies, including modification of mixture inhomogeneity, in a reasonable computational time. Furthermore, LEM has been used successfully in the past as a subgrid combustion model for large-eddy simulations, e.g., [6–8]. The results presented in this work suggest that LEM is a potential candidate as a submodel for CFD calculations of HCCI engines.

The paper is organized as follows: In the next section we introduce our modeling strategy using LEM. In Section 3 we compare results obtained with the LEM approach with some recent DNS data, and we finish in Section 4 with some concluding remarks.

2. Model formulation

The linear eddy model was proposed by Kerstein in [5] for nonreacting flow and extended to reactive flow in [9]. It has been discussed in detail in the literature, e.g., [5,9–12] and, therefore, is only briefly summarized here. The overall LEM concept for turbulent reactive flow consists of two concurrent processes representing the respective influences of dilatation-induced advection, molecular diffusion, chemical reactions, and turbulent transport. The first process is time advancement of the reactive zero-Mach-number equations in a one-dimensional domain resolving all spatial and temporal scales. The second process, turbulent transport, is implemented using a stochastic sequence of statistically independent stirring events.

2.1. The zero-Mach-number equations for reactive flow

We solve the variable-density zero-Mach-number equations in one spatial dimension on a fixed grid. The balance equations for species mass fractions and temperature are

$$\rho\frac{\partial Y_s}{\partial t}+\rho u\frac{\partial Y_s}{\partial x}=-\frac{\partial j_s}{\partial x}+M_s\dot{\omega}_s, \tag{1}$$

$$\rho c_\mathrm{p}\frac{\partial T}{\partial t}+\rho u c_\mathrm{p}\frac{\partial T}{\partial x}=\frac{dp}{dt}-\frac{\partial q}{\partial x}-\sum_s j_s\frac{\partial h_s}{\partial x}-\sum_s h_s M_s\dot{\omega}_s, \tag{2}$$

with $s=1,\ldots,n_s$ and n_s is the number of different species in the system. Here, ρ is the density, Y_s the mass fraction of species s, u the velocity, j_s the species diffusive flux, M_s the molecular weight of species s, $\dot{\omega}_s$ the chemical source term of species s, c_p the heat capacity at constant pressure, p the pressure, q the heat flux, and h_s the enthalpy of species s including the heats of formation. For the equation of state of a mixture of ideal gases we have

$$p = \rho T \sum_s Y_s R_s, \tag{3}$$

with R_s denoting the gas constant of species s.

In the zero-Mach-number limit the thermodynamic pressure p is spatially constant [13]. In this case a divergence constraint on the velocity can be derived from the energy equation [14]

$$\frac{\partial u}{\partial x} = -\frac{1}{\gamma p}\frac{dp}{dt} + \mathcal{U}, \tag{4}$$

where γ is the ratio of specific heats and $\mathcal{U}$ is given by

$$\mathcal{U} = -\frac{1}{\rho c_p T}\left\{\frac{\partial q}{\partial x} + \sum_s j_s \frac{\partial h_s}{\partial x}\right\} - \frac{1}{\rho}\sum_s \left\{\frac{M}{M_s}\frac{\partial j_s}{\partial x}\right\} + \frac{1}{\rho}\sum_s \left\{\frac{M}{M_s} - \frac{h_s}{c_p T}\right\}\dot{\sigma}_s.$$

Here M denotes the mean molecular weight of the mixture and $\dot{\sigma}_s = M_s \dot{\omega}_s$. Integrating (4) over the whole domain from $x = x_1$ to $x = x_1 + L$ results in an equation for the global pressure change,

$$\frac{dp}{dt} = \frac{\gamma p}{L}\left\{\int_{x=x_1}^{x_1+L} \mathcal{U}\, dx - (u_2 - u_1)\right\}. \tag{5}$$

For periodic or zero-velocity boundary conditions we have $u_1 = u_2$ and the last term in (5) vanishes. Under these conditions (the latter is used here; see Section 2.3), Eq. (5) allows us to calculate the pressure rise due to chemical reactions, heat conduction, and species diffusion. In the one-dimensional case, Eq. (4) allows the computation of the velocity by simple integration in space. Therefore it is not necessary to solve a momentum equation here. The velocity u in Eqs. (1), (2), and (4) represents the flow velocity induced by dilatational effects due to compression, conduction, and chemical reactions as given by (4).

It is important to note that similarly to a DNS, in the LEM concept Eqs. (1) and (2) need to resolve all spatial scales of a turbulent reacting flow.

2.2. Linear eddy mixing/turbulent transport

In the LEM concept, turbulent advection is implemented explicitly by stochastic eddy events. Each eddy event involves a rearrangement of all scalar quantities using so-called 'triplet maps.' The effect of a triplet map is a threefold compression of the scalar fields in a selected spatial interval whose size is denoted by l. This map increases the scalar gradients within the selected interval, analogous to the effect of compressive strain in turbulent flow, without creating discontinuities.

Two quantities are needed to specify an eddy event: eddy size l and eddy location within the domain. The eddy location is randomly sampled from a uniform distribution, and the eddy size is randomly sampled. Assuming the Kolmogorov inertial-range scaling the size distribution is given by [11]

$$f(l) = (5/3) l^{-8/3} / \left[\eta^{-5/3} - l_t^{-5/3}\right].$$

Using the turbulent Reynolds number

$$\mathrm{Re}_t = \frac{u' l_t}{\nu},$$

where ν is the kinematic viscosity, and u', l_t are the integral velocity and length scale, respectively, the Kolmogorov scale η is determined from the inertial scaling law

$$\eta = N_\eta l_t \mathrm{Re}_t^{-3/4}.$$

Here, N_η is an empirical constant.

Eddy events induce a random walk of fluid parcels whose diffusivity is the model analog to the turbulent diffusivity D_t. Based on this interpretation, the event frequency per unit length is determined by [11]

$$\lambda = \frac{54}{5}\frac{\nu \mathrm{Re}_t}{C_\lambda l_t^3}\frac{[(l_t/\eta)^{5/3} - 1]}{[1 - (\eta/l_t)^{4/3}]}.$$

The required model constants have been set to $C_\lambda = 15$ and $N_\eta = 10$. The value for C_λ has been adopted from [15]. Out of a few iterations with different values for N_η, this parameter set gave the best agreement with DNS heat release rates for the $T' = 15$ K case; see below. Calibration of this type is always necessary in LEM; e.g., in [11] N_η has been tuned to match the high-wavenumber cutoff of scalar power spectra. More careful tuning might lead to further improvement of the results. However, it should be pointed out that this tuning of parameters needs to be done only once for some model configuration. Once a suitable parameter set has been determined, the model should be applicable for any other operating conditions. Model applicability over a range of T' values based on the calibration at $T' = 15$ K is demonstrated here, showing that the model, with the assigned parameter values, has predictive capability.

2.3. Numerical implementation

The zero-Mach-number equations are solved numerically using standard second-order finite-difference discretization. No-flux boundary conditions are applied, hence $u_1 = u_2 = 0$. Periodic boundary conditions, consistent with the DNS comparison case, will be applied in the future. Results thus far indicate that this change will have negligible effect, especially for those cases where we use a LEM domain size much larger than the size of the DNS domain; see Section 3.3.

Table 1
Lewis numbers for all species

	H_2	O_2	O	OH	H_2O	H	HO_2	H_2O_2	N_2
Le_s	0.32	1.15	0.75	0.76	0.84	0.19	1.16	1.16	1.00

The time integration of the stiff set of equations is performed using the DAE solver IDA of the SUNDIALS package [16]. In order to not destroy the band structure of the sparse solver, no-flux boundary conditions are applied for all variables. Periodic boundary conditions, consistent with the DNS comparison case, would require major changes in the IDA solver.

Thermodynamic and transport properties as well as reaction rates are calculated using the C++ interface of the CANTERA software package [17].

3. Results

3.1. Initial conditions

We test the LEM approach against DNS results presented in [2]. The 2D DNS results were obtained on a domain of size 4.1 mm in each spatial direction with a uniform grid spacing of 4.3 μm and periodic boundary conditions. The initial conditions of the turbulent flow field in the DNS were prescribed by an initial turbulent kinetic energy spectrum of Passot–Pouquet type and a similar random temperature field superimposed on a mean temperature. Beside the obvious differences between a 1D (LEM) and a 2D (DNS) model, the following set of parameters and initial conditions of the LEM are identical to the DNS in [2].

The equivalence ratio of the initially homogeneous H_2–air mixture is $\phi = 0.1$ in all cases. Initial pressure and temperature are $p_0 = 41$ atm and $T_0 = 1070$ K, respectively. The calculated ignition delay time for a homogeneous mixture under these conditions is $t_{ig} = 2.9$ ms and the peak heat release rate is $hr_0 = 2.9408\ \mathrm{MJ/m^3/s}$. The detailed chemical mechanism for H_2–air chemistry has been taken from [18] and uses 8 reactive species (see Table 1) and 21 reversible reactions. The diffusion coefficients are calculated in accordance with the DNS from the prescribed Lewis numbers Le_s shown in Table 1. Transport coefficients are evaluated as mixture averaged values and all thermodynamic quantities are evaluated from the well-known NASA polynomials using CANTERA's built-in routines. To evaluate model sensitivity to turbulent transport, cases with $Le_s = 1$ for all species s are also reported.

The initial conditions correspond to a compression ratio of 15:1 starting at 1 atm and 400 K. Decoupling the compression stage from the ignition stage is justifiable for hydrogen/air chemistry, which exhibits very low heat release rates at lower temperatures. However, such an approximation is inadequate for more realistic fuels such as n-heptane with multistage ignition behavior. These parameters have been argued in [2] to be representative for engines operating at low load. Due to the relatively low equivalence ratio and the moderate compression rate it can be safely assumed that developing compressive waves such as shocks and detonations are not present [2].

Integral turbulent length and velocity scales for the LEM runs are taken from the DNS and are $l_t = 0.34$ mm and $u' = 0.5$ m/s. A random temperature field with a Passot–Pouquet spectrum [19]

$$E(k) = \frac{32}{3}\sqrt{\frac{2}{\pi}}\frac{T'^2}{k_e}\left(\frac{k}{k_e}\right)^4 \exp\left(-2\left(\frac{k}{k_e}\right)^2\right) \qquad (6)$$

is superimposed on the mean temperature field to specify initial temperature inhomogeneities. Here, k is the wave number, k_e is the most energetic wave number defined by $k_e = 2\pi/l_e$, and T' is the RMS temperature fluctuation. The resulting initial temperature field is

$$T(x) = T_0 + \sum_{k=1}^{\infty}(\Delta T)_k \sin(2\pi k x/L + \phi_k), \qquad (7)$$

where T_0 denotes the initial mean temperature, and ϕ_k is the randomly chosen phase of mode k with $0 \leqslant \phi_k \leqslant 2\pi$. The temperature amplitude at wavenumber k for a periodic temperature field with a discrete spectrum is given by

$$(\Delta T)_k = \left(2\int_{k-1/2}^{k+1/2} E(k)\,dk\right)^{1/2} \approx \big(2E(k)\big)^{1/2}.$$

With this initialization the resulting initial temperature field has exactly the prescribed RMS value T'.

In accordance with the DNS, the most energetic length scale is $l_e = 1.32$ mm. The initial velocity RMS is $v' = 0.5$ m/s and the initial autocorrelation integral length scale is $l_t = 0.34$ mm. This leads to a turbulent Reynolds number of $Re_t = 45$. The characteristic integral time scale can be estimated by $t_t = l_t/v' = 0.68$ ms, which is of the same order of magnitude as the homogeneous ignition delay time $t_{ig} = 2.9$ ms and therefore allows for strong interactions between turbulence and chemistry.

All LEM simulations in this study have been run with a uniform grid spacing of 4.3 μm taken from the DNS. This grid spacing has been reported in [1] to be necessary and sufficient to resolve ignition fronts under the given conditions.

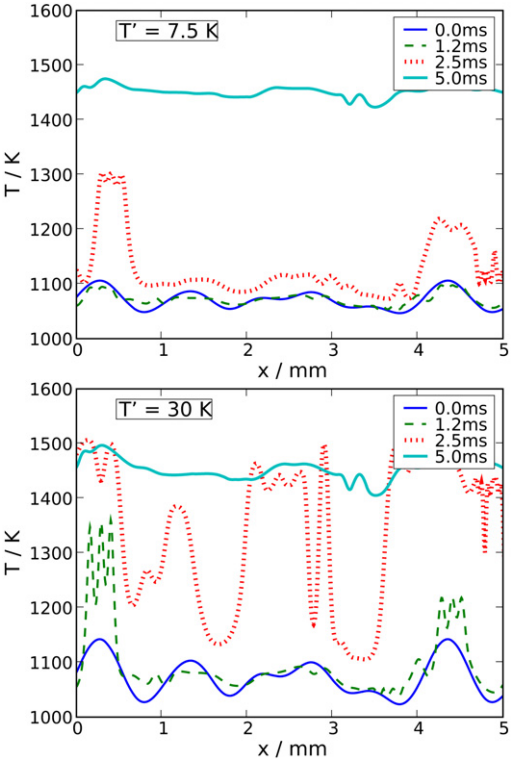

Fig. 1. Temperature profiles at different times for initial temperature RMS values of $T' = 7.5$ and 30 K.

3.2. Spatial structure of ignition

For a qualitative picture of the spatial structure of a typical ignition event, Fig. 1 shows temperature profiles at different times for $T' = 7.5$ and 30 K. The low fluctuations in the first case lead to almost homogeneous autoignition with only two moderate hot spots advancing ahead of an almost homogeneous region in between. From the $T' = 30$ K case it becomes obvious that the large initial temperature fluctuations induce locally different ignition delays between initial minimum and maximum values resulting in large temperature gradients. These temperature gradients are subject to turbulent mixing during the "delay time window."

3.3. Domain size influence

In order to get meaningful statistics within the LEM approach, it is necessary either to perform many different realizations on a LEM domain with a linear dimension comparable to the DNS, or to run a single calculation on a domain much larger than the spatial extent of the two-dimensional DNS of Chen et al. [1], which is $l_{\mathrm{DNS}} \times l_{\mathrm{DNS}}$ with $l_{\mathrm{DNS}} = 4.1$ mm. Here we follow the second approach. Fig. 2 shows heat release

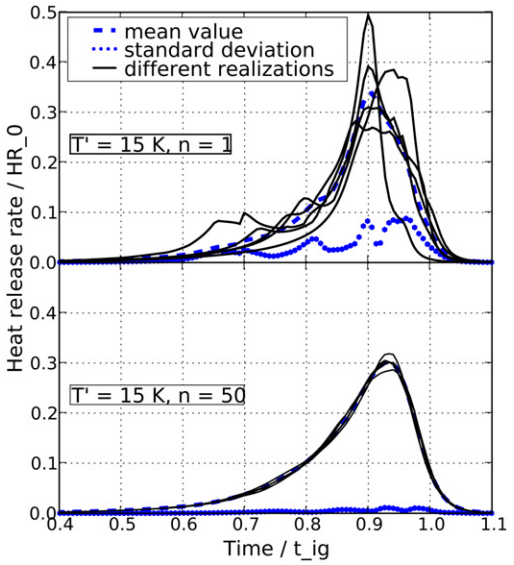

Fig. 2. Influence of LEM domain size on heat release rates. Solid lines represent different realizations, dashed lines the mean value, and dotted lines the standard deviation of those realizations. The size of the LEM domain is $l_{\mathrm{LEM}} = n l_{\mathrm{DNS}}$.

rates as a function of time for different initial random temperature distributions with an initial temperature fluctuation of $T' = 15$ K as well as mean value and standard deviation of those realizations. Time and heat release rates have been made nondimensional by the ignition delay time $t_{\mathrm{ig}} = 2.9$ ms and the peak heat release rate $hr_0 = 2.9408\ \mathrm{MJ/m^3/s}$ of the homogeneous reactor, respectively. In the top graph of Fig. 2 the LEM domain is $l_{\mathrm{LEM}} = l_{\mathrm{DNS}}$, corresponding exactly to the spatial extent of the DNS. It is obvious that different initial conditions lead to very different heat release rates over time. The standard deviation at the time of peak heat release of the mean for the case with $l_{\mathrm{LEM}} = l_{\mathrm{DNS}}$ is approximately 20%. The bottom graph of that figure shows heat release rates with five different random initial conditions with a spatial domain $l_{\mathrm{LEM}} = 50 l_{\mathrm{DNS}}$. Each calculation can be interpreted as a representation of 50 different realizations of initial conditions with $l_{\mathrm{LEM}} = l_{\mathrm{DNS}}$. We note that different random seeds have been used in each calculation for implementation of the LEM stirring events. The standard deviation for this set of realizations is always less than 4%. At the time of peak heat release of the mean, the standard deviation is 3.5%. Based on the heat release rates versus time and the small deviations between the five different calculations, we suppose that 50 realizations or an LEM domain of 50 times the DNS domain size gives reasonable statistical results for this study. All results presented below use a LEM domain $l_{\mathrm{LEM}} = 50 l_{\mathrm{DNS}}$. With a grid spacing of 4.3 μm and a domain size of

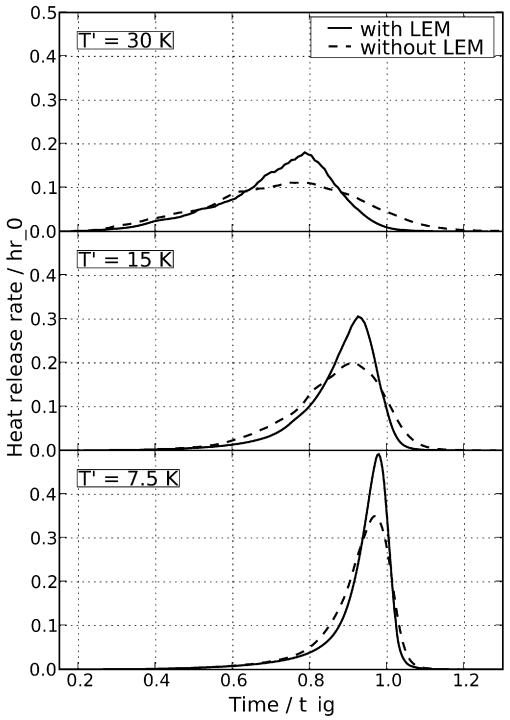

Fig. 3. Influence of turbulence on heat release rates. Curves labeled "without LEM" have been obtained by switching off the LEM triplet maps.

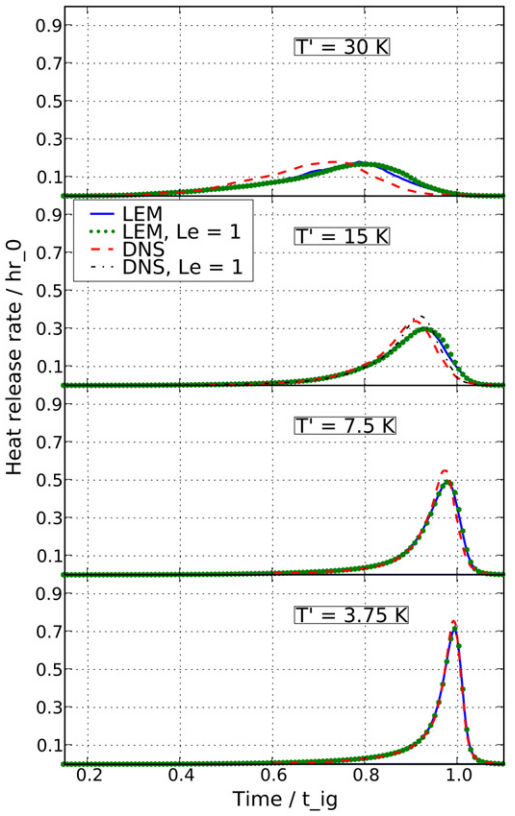

Fig. 4. LEM and DNS heat release rates versus time for different initial temperature fluctuations. LEM results are shown for cases with $Le_s \neq 1$ and $Le_s = 1$; DNS results with $Le_s \neq 1$ are taken from [2]. DNS data with $Le_s = 1$ are only available for $T' = 15$ K and are taken from [3].

$l_{LEM} = 50 l_{DNS} = 204$ mm, the total number of grid points for the LEM was roughly 48,000. Computational times with this domain size and grid resolution were on the order of 12–16 h on a G5 processor running at 2 GHz. As BDF-type methods such as the used IDA solver require a time-consuming startup after each LEM stirring event, further significant runtime improvements can be expected using, e.g., implicit Runge–Kutta methods.

3.4. Heat release rates

The principal influence of initial temperature fluctuations and turbulent mixing is shown in Fig. 3. During the initial ignition stage the influence of turbulence is almost negligible. However, during the phase of peak heat release, turbulence cannot be neglected. In all cases, turbulence leads to increased peak heat release rates. This is due to the fact that turbulence tends to homogenize the initial temperature fluctuations, bringing heat release rates closer to the homogeneous reactor case with its typical explosion behavior for reactions with high activation energy. Fig. 3 shows that both initial temperature fluctuations and turbulent mixing have a distinct influence on heat release rates under HCCI conditions.

Fig. 4 shows heat release rates over time for different initial T' values. With increasing T', the heat release is spread over a longer time period. Reasonable agreement is obtained between the DNS results of Hawkes et al. [2] and LEM for temperature fluctuations $T' = 3.75$, 7.5, and 15 K, although less so as T' increases. In addition to the LEM results obtained with different but constant Lewis numbers, Fig. 4 also shows LEM results for the unity-Lewis-number case. For the initial temperature fluctuations under consideration, it is shown below that the influence on the H_2 budget terms is significant, but Fig. 4 indicates that the influence of the Lewis number on heat release rates is marginal.

The only $Le_s = 1$ DNS comparison data, reported in [3], are for $T' = 15$ K. A slight late-time stretching of the heat-release profile relative to the $Le_s \neq 1$ DNS case is seen. LEM indicates the same sensitivity. A more complete set of DNS $Le_s = 1$ results would allow a further evaluation of LEM molecular transport

sensitivities. (This aspect of LEM has been examined in several previous studies [20–22].)

Besides the obvious conceptual differences between the one-dimensional LEM and the two-dimensional DNS, there are some other important differences here. Whereas the DNS represents decaying turbulence, the LEM as implemented here mimics a constant turbulence level. The tuning of N_η described in Section 2.2 enforces overall conformance of LEM to DNS mixing properties. For present purposes, it is not necessary to match mixing properties in finer detail, but it could be useful in future studies. In addition, LEM is formulated to represent the 3D inertial-range cascade (Section 2.2 and cited references), but 2D DNS has different cascade physics and scalings. Finally, the LEM calculations with domain size $l_{\mathrm{LEM}} = 50 l_{\mathrm{DNS}}$ can be—to a certain degree, see Section 3.3—regarded as statistically convergent, whereas each DNS result corresponds to a single representation of the process. Despite these differences between models, the LEM is able to produce heat release rates that are qualitatively and quantitatively comparable to DNS results.

3.5. Mean reaction-front speed

Zel'dovich [23] distinguished five different combustion modes in a homogeneous mixture with a nonhomogeneous initial temperature distribution: (i) near-instantaneous thermal explosions, (ii) conventional deflagration waves, (iii) developing detonation waves, (iv) subsonic, and (v) supersonic autoignitive spontaneous ignition fronts driven by a nonuniform distribution of ignition delay times corresponding to temperature inhomogeneities. These different regimes have been identified in [24] by comparing the initial temperature gradient to the critical temperature gradient of a hot spot leading to a sonic reaction-front speed.

A definition for a density-weighted displacement speed capable of representing all regimes between the spontaneous ignition-front propagation (where molecular transport is negligible) and the deflagration wave has been derived in [25]. In one spatial dimension this displacement speed is given by the density-weighted material derivative of a scalar ϕ at a fixed value $\phi^\star$,

$$s_{\mathrm{d}}^\star = \frac{\rho}{\rho_{\mathrm{u}}} \frac{D\phi^\star}{Dt} \left(\frac{d\phi}{dx} \right)^{-1}_{\phi=\phi^\star},$$

where ρ_{u} is a representative density of the reactants at the local conditions that can be calculated from the local enthalpy and the unburned mixture composition assuming constant pressure. With $\phi = Y_{\mathrm{H_2}}$ and replacing the material derivative with the transport equation for the species mass fraction (1), we can write

$$s_{\mathrm{d}}^\star = -\frac{1}{\rho_{\mathrm{u}}} \left\{ \frac{dj_{\mathrm{H_2}}}{dx} - M_{\mathrm{H_2}} \dot{\omega}_{\mathrm{H_2}} \right\} \left(\frac{dY_{\mathrm{H_2}}}{dx} \right)^{-1}_{Y_{\mathrm{H_2}}=Y^\star_{\mathrm{H_2}}}. \quad (8)$$

For a steady planar deflagration wave without heat loss the density-weighted displacement speed is constant over the flame structure. This definition has been used in the DNS study [1,2] as an indicator for identifying different combustion regimes and will be used here as well. As a reference value for tracking the front, a value of $Y^\star_{\mathrm{H_2}} = 8.5 \times 10^{-4}$ has been used [1]. This value corresponds approximately to the value at maximum heat release.

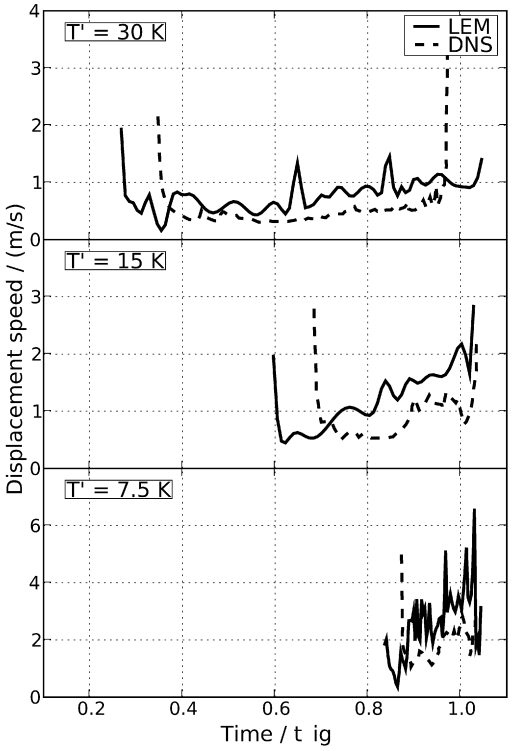

Fig. 5. Displacement speed over time for LEM and DNS [2]. LEM displacement speeds are arithmetic mean values of all reaction fronts identified in the domain.

Fig. 5 shows displacement speeds over time for different initial temperature fluctuations and compares LEM results with DNS results taken from [2]. We remark that the LEM displacement speeds shown in Fig. 5 are arithmetic mean values of all displacement speeds at a given time observed within the LEM domain. The LEM calculations in Fig. 5 show the same qualitative U shape as the DNS. The minimum speed decreases with increasing temperature fluctuations T' and the quantitative values obtained with LEM and DNS are of the same order of magnitude. Because LEM values are averages over individual,

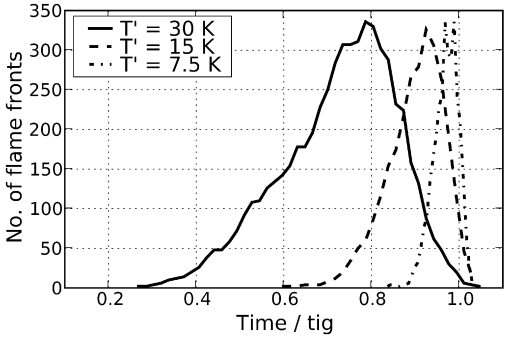

Fig. 6. Number of flame crossings for evaluation of displacement speeds in Fig. 5.

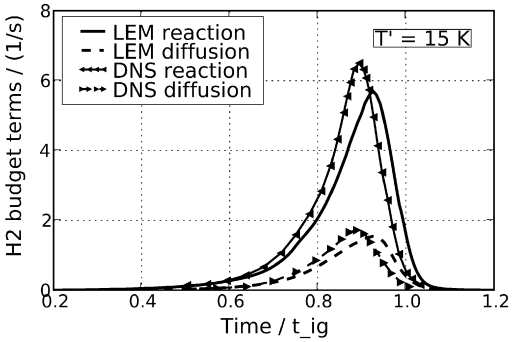

Fig. 7. LEM and DNS [2] spatially averaged H_2 diffusion and reaction budget terms.

separately propagating reaction zones but DNS values are averages over smooth isocontours, LEM results are more intermittent than the DNS. The laminar flame speed under the local conditions is on the order of 40–50 cm/s; see Fig. 3 of [1]. From Fig. 5 it becomes obvious that the observed displacement speed for the $T' = 30$ K case is mostly in the vicinity of the laminar flame speed, indicating the importance of both reaction and diffusion in this regime. With decreasing temperature fluctuations the observed displacement speeds increase in accordance with the expectation that with decreasing molecular transport the front speed increases toward the displacement speeds of the spontaneous ignition-front propagation.

Fig. 6 shows the number of identified flame fronts over time used to calculate the mean values in Fig. 5. These data provide a rough indication of the standard deviation of the displacement speeds plotted in Fig. 5 based on $n^{-1/2}$ scaling of the ratio of the standard deviation to the mean, where n is the number of displacement-speed values used to compute the mean.

3.6. Budget terms

The relative importance of diffusion and the chemical source term for hydrogen mass fraction is shown in Fig. 7 for an initial temperature fluctuation of $T' = 15$ K. Consistent with the heat release rates for the $T' = 15$ K case in Fig. 4, the profiles of the LEM simulation lag in time behind the DNS data with a slightly lower peak reaction term in the LEM simulation. The DNS data are taken from Fig. 15 of [1], and for the diffusion term, the absolute value has been taken for comparison. Again, the overall agreement between the LEM and the DNS is quite reasonable here. At peak heat release the H_2 reaction term equals 5.71 s^{-1} and the diffusion term 1.54 s^{-1}, which corresponds to 27% of the reaction term. This value is in excellent agreement with the DNS value of 27% reported in [1]. Whereas Fig. 7 shows a quantitative comparison of spatially averaged H_2 reaction and diffusion budget terms between LEM and DNS, Fig. 8 shows the budget terms for different initial temperature fluctuations. For $T' = 3.75$ K the molecular diffusion term is negligible compared to the chemical source term. With increasing initial temperature fluctuations, the relative importance of the diffusion term increases. At $T' = 15$ K the diffusion and source terms are of the same order of magnitude, which is typical for propagating flame fronts. In accordance with the discussion given in Section 3.5, Fig. 8 indicates different combustion modes ranging from ignition-front propagation to deflagration-like combustion waves.

Using hydrogen as a fuel, one might expect strong differential diffusion influence. It has been shown in Fig. 4 that differential diffusion effects have a marginal influence on heat release rates under the conditions considered in this study. Fig. 9 compares spatially averaged H_2 diffusion and reaction budget terms with and without differential diffusion effects. The influence of differential diffusion effects on the H_2 reaction budget term is—in accordance with the heat release rates—small. The H_2 diffusion budget terms are, however, strongly influenced by differential diffusion. For the cases with $T' = 15$ K and 30 K shown in Fig. 9, the absolute value of the diffusion budget term with differential diffusion is about twice as large as without.

Another indicator of different combustion modes under HCCI conditions can be obtained from the PDF of the ratio of diffusion and reaction budget terms. In [3], PDFs of this ratio based on the DNS of [2] have been presented. Fig. 10 shows the corresponding PDFs for the LEM. In accordance with [2], the PDFs have been computed at the time of maximum heat release and an isolevel $Y_{H_2} = 0.00033$. From Fig. 10 it can be observed that with increasing initial temperature fluctuations the PDFs becomes broader, indicating the increased importance of the diffusion relative to the chemical source term. For $T' = 3.75$ K, the PDF shows a narrow profile with

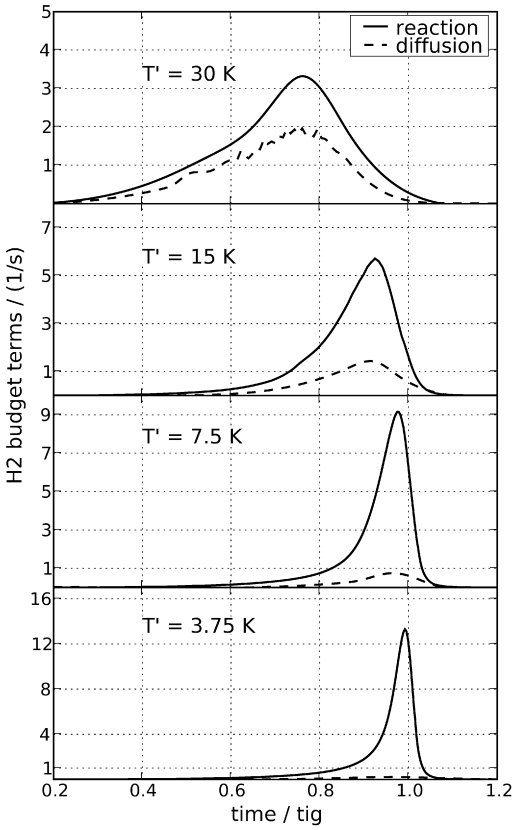

Fig. 8. LEM spatially averaged H_2 diffusion and reaction budget terms.

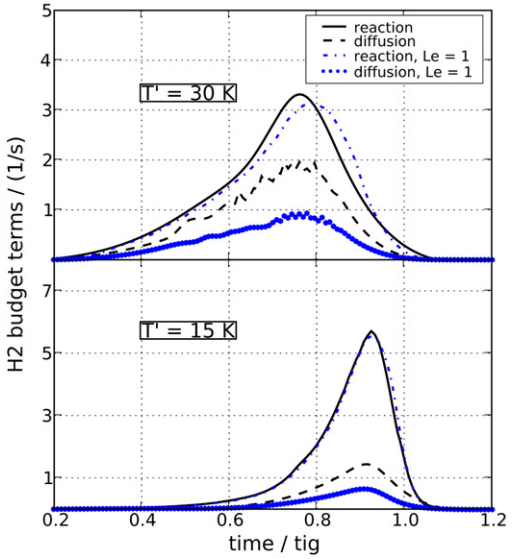

Fig. 9. LEM spatially averaged H_2 diffusion and reaction budget terms for $\mathrm{Le_s} \neq 1$ and $\mathrm{Le_s} = 1$ and initial temperature fluctuations of $T' = 15$ and $T' = 30$ K.

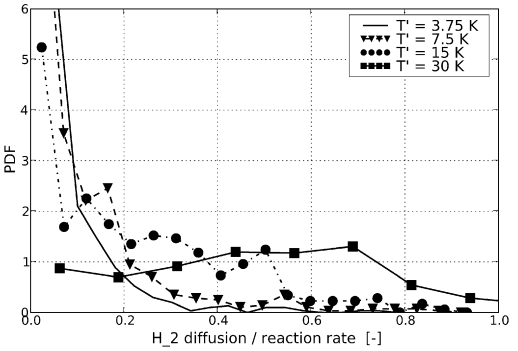

Fig. 10. PDF of the diffusion-to-reaction-budget-term ratio for the H_2 mass fraction constrained to the peak heat release and a value of $Y_{H_2} = 0.00033$.

a peak value at zero ratio corresponding to negligible diffusion in this case. For $T' = 30$ K the PDF has a broad profile for ratios up to approximately 0.7. Despite some quantitative differences between the LEM PDF in Fig. 10 and the DNS PDF presented in [3], some key features of the DNS PDFs are reproduced by the LEM: A monotonic decrease of the PDF for $T' = 3.75$ K and 7.5 K, a shoulder that extends to about 0.5 (about 0.6 in the DNS) for $T' = 15$ K, and a slight upward trend peaking at about 0.7 for $T' = 30$ K. Compared to the DNS PDF for $T' = 30$ K in [3], the LEM PDF falls off more gradually after the peak at 0.7. LEM has occasionally higher gradients than DNS, reflecting LEM conformance to the intermittency properties of 3D turbulence [11] vs the less intermittent nature of 2D turbulence. (In this regard, 3D DNS would be a more direct comparison case.) This leads to stronger diffusion terms and extends the PDF to higher values in the sample space compared to the DNS. The PDF results further illustrate the progression, with increasing T', from ignition-front propagation through a mixed regime and then toward deflagration-like combustion in the LEM simulations as well as the DNS.

4. Conclusions

We have presented an application of the linear eddy model for the simulation of autoignition under thermal stratification for HCCI-like conditions. A detailed hydrogen chemical mechanism has been used. We compared LEM results with recent DNS data. The predicted heat release rates, as well as the relative importance of reaction and diffusion terms, agree qualitatively and quantitatively reasonably well with the DNS results. The simple one-dimensional LEM is capable of capturing the key combustion characteristics for the combustion regime of sponta-

neous ignition fronts, for the deflagration-dominated case, and last for the mixed one. The comparisons to DNS do not constitute a validation of the LEM simulations because the DNS, being 2D, is itself a model rather than a quantitatively accurate flow simulation, including, e.g., different intermittency features. The relationship between the two methods is that they both advance the spatially and temporally resolved diffusion and reaction processes and both involve idealized (relative to 3D turbulence) representations of advection, where the nature of the idealization is different in the two methods. The consistency of the results obtained using the two methods suggests that the salient features of the combustion regime considered here are insensitive to the details of advection modeling. Nevertheless, validation by means of eventual comparison with 3D DNS would be useful to validate either of these approaches (2D DNS, LEM).

The 1D strategy of LEM enables parametric studies, including modification of mixture inhomogeneity, in a reasonable computational time. Despite the limitation of being 1D only, it is especially this feature that allows the investigation of turbulent Reynolds numbers regimes that are not accessible by 2D or 3D DNS. The results presented in this work suggest that LEM is a potential candidate as a submodel for CFD calculations of HCCI engines.

Acknowledgments

The authors acknowledge the support and helpful discussions with J. Chen and E. Hawkes.

This work was partially supported by the Division of Chemical Sciences, Geosciences, and Biosciences, Office of Basic Energy Sciences, United States Department of Energy, and by the National Science Foundation under Grant No. ATM-0346854. Sandia National Laboratories is a multi-program laboratory operated by Sandia Corporation, a Lockheed Martin Company, for the United States Department of Energy under contract DE-AC04-94-AL85000.

References

[1] J.H. Chen, E.R. Hawkes, R. Sankaran, S.D. Scott, H.G. Im, Combust. Flame 145 (2006) 128–144.
[2] E.R. Hawkes, R. Sankaran, P.P. Pebay, J.H. Chen, Combust. Flame 145 (2006) 145–159.
[3] D.J. Cook, H. Pitsch, J.H. Chen, E.R. Hawkes, Proc. Combust. Inst. 30 (2006) 2903–2911.
[4] R. Steeper, V. Sankaran, J. Oefelein, Simulation of the effect of spatial fuel distribution using a linear-eddy model, SAE Technical Paper Series 2007-01-4131.
[5] A.R. Kerstein, Combust. Flame 75 (1989) 397–413.
[6] V.K. Chakravarthy, S. Menon, Flow Turb. Combust. 65 (2000) 133–161.
[7] V.K. Chakravarthy, S. Menon, Combust. Sci. Technol. 162 (2001) 175–222.
[8] V. Sankaran, S. Menon, Proc. Combust. Inst. 30 (2005) 575–582.
[9] A.R. Kerstein, Combust. Sci. Technol. 81 (1992) 75–96.
[10] A.R. Kerstein, Combust. Sci. Technol. 60 (1988) 391–421.
[11] A.R. Kerstein, J. Fluid Mech. 231 (1991) 361–394.
[12] A.R. Kerstein, J. Fluid Mech. 240 (1992) 289–313.
[13] R. Klein, J. Comput. Phys. 121 (1995) 213–237.
[14] M.S. Day, J.B. Bell, Combust. Theory Model. 4 (2000) 535–556.
[15] V. Sankaran, S. Menon, Proc. Combust. Inst. 28 (2000) 203–209.
[16] A.C. Hindmarsh, Sundials: Suite of Nonlinear and Differential/Algebraic Equation Solvers, Tech. Rep. UCRL-JRNL-200037, Lawrence Livermore National Laboratory, 2004.
[17] D. Goodwin, CANTERA: Object-Oriented Software for Reacting Flows, http://www.cantera.org.
[18] M.A. Mueller, T.J. Kim, R.A. Yetter, F.L. Dryer, Int. J. Chem. Kinet. 31 (1999) 113–125.
[19] J.O. Hinze, Turbulence, McGraw–Hill, 1975.
[20] A.R. Kerstein, J. Fluid Mech. 216 (1990) 411–435.
[21] A.R. Kerstein, M.A. Cremer, P.A. McMurtry, Phys. Fluids 7 (1995) 1999–2007.
[22] V. Nilsen, G. Kosaly, Phys. Fluids 9 (1997) 3386–3397.
[23] Y.B. Zel'dovich, Combust. Flame 39 (1980) 211–214.
[24] X.J. Gu, D.R. Emerson, D. Bradley, Combust. Flame 133 (2003) 63–74.
[25] T. Echekki, J.H. Chen, Combust. Flame 118 (1999) 308–311.